

NbTi/Nb/Cu multilayer shield for the superconducting shield (SuShi) septum

D. Barna*[†], M. Novák*, K. Brunner*, C. Petrone[‡], M. Atanasov[‡], J. Feuvrier[‡], M. Pascal[‡]

*MTA Wigner Research Centre for Physics, Budapest

[†]barna.daniel@wigner.mta.hu

[‡]CERN, Geneva

Abstract—A passive superconducting shield was proposed earlier to realize a high-field (3-4 T) septum magnet for the Future Circular Collider. This paper presents the experimental results of a potential shield material, a NbTi/Nb/Cu multilayer sheet. A cylindrical shield was constructed from two halves, each consisting of 4 layers with a total thickness of 3.2 mm, and inserted into the bore of a spare LHC dipole corrector magnet (MCBY). At 4.2 K, up to about 3.1 T at the shield's surface only a leakage field of 12.5 mT was measured inside the shield. This can be attributed to the mis-alignment of the two half cylinders, as confirmed by finite element simulations. With a better configuration we estimate the shield's attenuation to be better than 4×10^{-5} , acceptable for the intended application. Above 3.1 T the field penetrated smoothly. Below that limit no flux jumps were observed even at the highest achievable ramp rate of more than 50 mT/s at the shield's surface. A 'degaussing' cycle was used to eliminate the effects of the field trapped in the thick wall of the shield, which could otherwise distort the homogeneous field pattern at the extracted beam's position. At 1.9 K the shield's performance was superior to that at 4.2 K, but it suffered from flux jumps.

Index Terms—superconducting shield, NbTi, septum magnet, Future Circular Collider, accelerator

I. INTRODUCTION

The Future Circular Collider (FCC) study was launched in 2014 to identify the key challenges of the next-generation particle collider of the post-LHC era, propose technical solutions and establish a baseline design. In its early phase the parameters are subject to frequent changes. The current values of the relevant parameters are shown in Table I. One of the key problems of the proton-proton ring is the high beam rigidity and the very strong magnetic fields required to manipulate this beam. A new generation of superconducting dipole magnets using Nb₃Sn conductors is being developed to produce the 16 T field necessary to keep the beam on orbit. The beam extraction system uses so-called septum magnets, which create zero field at the position of the circulating beam, and a high field region in close proximity for the extracted beam kicked off-orbit by upstream kicker magnets. The unprecedented beam rigidity (a factor of 6.6 higher than in today's highest-energy ring, the LHC) puts serious requirements on these magnets as well. A magnetic field of at least 3 T is desired in order to keep the total length of the septa within limits, and the apparent septum thickness (total thickness of all

TABLE I
RELEVANT PARAMETERS OF THE FUTURE CIRCULAR COLLIDER

Parameter	Symbol	Value	Unit
Circumference		80-100	km
Collision energy		50+50	TeV
Injection energy		1.3/3.3	TeV
Septum field homogeneity		± 1.5	%
Septum integrated field	$\int B dl$	190	Tm
Deflection by the septa	α_s	1.14	mrad
Deflection by the kickers	α_k	0.13	mrad
Maximum apparent septum thickness		25	mm

materials, including beam pipes and beam screens between the two regions) needs to be minimized in order to relax the requirements on the kicker magnets' strength. The target value is 25 mm, which corresponds to a thickness of 17-18 mm of the shield itself, without beam pipes and beam screens. These lead to a very sharp transition between the high-field and no-field regions of the septa. These requirements are even more important for the high-energy LHC (HE-LHC) option (an alternative to the FCC), which would use FCC technology in the LHC tunnel, where space is very limited.

In a recent proposal [1] this field configuration would be realized by the combination of a superconducting magnet and a passive superconducting shield, referred to as a superconducting shield (SuShi) septum in the following. The geometry of the shield and the magnet winding need to be optimized simultaneously to give the required field homogeneity outside the shield. While a complete demonstrator prototype creating this homogeneous field pattern would be a major project including the design and construction of a special superconducting magnet, different superconducting shield materials can be easily tested in simpler setups and existing magnets. These tests can study the performance of the shield materials in general, with special focus on the following points: (i) Maximum shielded field with a given thickness. This defines the apparent septum thickness of the septum magnet for a given magnetic field. (ii) Stability against flux jumps, which lead to the sudden collapse of the shielding currents and the penetration of the magnetic field to the circulating beam. Besides an immediate beam abort, the shield would need to be heated above its critical temperature and cooled back in zero field ("thermal reset") in order to eliminate the trapped field. This is a very long process, leading to unacceptably long deadtimes. The shield itself must be stable against spontaneous flux jumps,

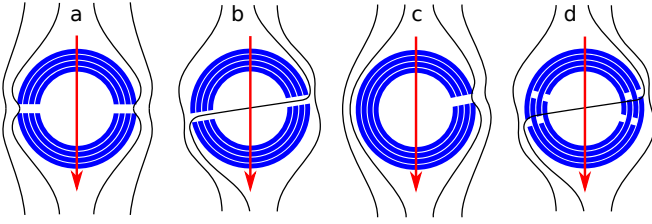


Fig. 1. Different cylindrical shield configurations made from a sheet material, and alignment errors. The vertical red arrows indicate the direction of the external dipole field of the MCBY magnet in the absence of the shield. Black lines indicate induction lines schematically in the presence of the shield. (a) Ideal alignment of two half-cylinders with respect to an external dipole field. (b) Mis-aligned arrangement of two half-cylinders. (c) Mis-aligned arrangement of concentric C-shape elements. (d) Zig-zag arrangement of half cylinders.

and external perturbations such as energy depositions due to beam loss must be minimized in the accelerator at this position. (iii) The septum magnet must be ready to a beam abort at any time, i.e. its field level must follow the actual beam momentum in the ring, from injection to top energy. The shield must therefore safely support repeated magnetic cycles between injection and top energy field levels, without flux jumps. (iv) A detection mechanism is needed to detect a developing flux jump safely before the field level starts to rise at the position of the circulating beam, so that the beam can be aborted. With a 100 km circumference of the ring the full revolution time is 333 μs . This is the minimum time requirement for an advance trigger to synchronize the extraction with the next abort gap. Including other delays, a safe time interval is a few milliseconds at least. (v) Even if the field does not penetrate to the interior of the shield at all, a trapped magnetic field will remain in its thick wall after a high field exposure, which will distort field homogeneity, most significantly at low external field levels, i.e. at injection into the ring. Elimination of this trapped field by a thermal reset is not possible due to downtime reasons, as argued above. The tests must demonstrate other possibilities.

The results presented in this paper are an extension of the work carried out by [2] with a different shield configuration that is suitable for constructing a septum magnet, and addressing further issues not studied in that paper.

II. EXPERIMENTAL SETUP

A cylinder of length $L=450$ mm, inner/outer diameter 41/47.4 mm was constructed from two half cylinders, each consisting of 4 layers of a 0.8 mm thick NbTi/Nb/Cu multilayer sheet [2], [3]. This material was used earlier for the construction of the inflector magnet for the BNL $g-2$ experiment [4], and to create a magnetic field concentrator [5]. The sheet is the discontinued proprietary product of Nippon Steel Ltd. Similar sheets are currently not available from other vendors. The aim of this experiment was to confirm the excellent shielding properties reported in [2], and test further aspects which are important for its application in a SuShi septum magnet. Material R&D is beyond the scope of the SuShi septum project, and therefore a semi-finished

sheet was purchased from the remaining stock of the company, and post-processed by the developer engineer of the sheet in a private company in Japan. Public information about the manufacturing process is described in [2], [3] and summarized below. The sheet was manufactured by packing NbTi and Cu sheets alternately into a copper box, interleaved with thin Nb sheets at each interface. The box was closed by electron beam welding under vacuum, and then hot rolled, cold rolled and heat treated. The final thickness of the 30 NbTi layers is around 9.5 μm . The Cu layers have the same thickness, except the two outermost ones being 95 μm thick. The thickness of the Nb layers is 0.95 μm , and their role was to prevent the diffusion of Ti into Cu during the heat treatment. The NbTi sheets were manufactured by hot forging, hot rolling and cold rolling of a commercially available Nb-46.5wt%Ti ingot. Commercially available four-9 OFHC copper (estimated RRR=100) was used for the Cu sheets. Parameters of the heat treatment have an important effect on the critical current density of the material, as reported in [3], [6]. The filling factor of the composite by NbTi is about 36%. The resulting multi-layer structure is a 2D analogue of the standard superconductor cables, where superconducting filaments are embedded typically in a copper matrix. The NbTi layers are responsible for the high current densities and thereby the shielding performance of the material, and Cu is used for stabilization.

Figures 1(a-d) show different cylindrical shield configurations for a transverse dipole field which can be made from a sheet material. With two half cylinders aligned perfectly with respect to the external field (a) the shielding currents do not cross the plane of the cut, and the leaking magnetic field inside the shield is parallel to the external field. If the shield is slightly misaligned (b), induction lines can pass through the two cuts and the major component of the leak field will be perpendicular to the external field. This effect is eliminated and the shielding efficiency is made less sensitive to misalignments if the shield is made from concentric C-shape elements as shown in Fig. 1(c). An alternating arrangement of the cuts on the left and right sides of configuration (c) is even better. Even though the configuration (c) was planned initially, the sheets were accidentally cut to half without excess material, which finally only allowed the realization of the two half-cylinders configuration (b), without the possibility to machine the meeting sides of the half cylinders to a flat surface. A further possible configuration with half-cylinders is illustrated in Fig. 1(d). Whether this arrangement improves the shielding efficiency with respect to configuration (b) is a function of the degree of misalignment of the latter. Although configuration (d) seems to be symmetric in average, the subsequent layers from inside to outside are exposed to an increasing magnetic field, and therefore the effects of their rotations have different weights, leading to the schematic field pattern shown in the figure, confirmed by finite element simulations. Although for large enough misalignments of configuration (b) the configuration (d) could perform better, our strategy was to assemble configuration (b) with the best possible alignment. Mounting configuration (d) would also have been difficult due to the spring-back effect of the shells. In the final setup there remained small gaps between the two half-cylinders. In

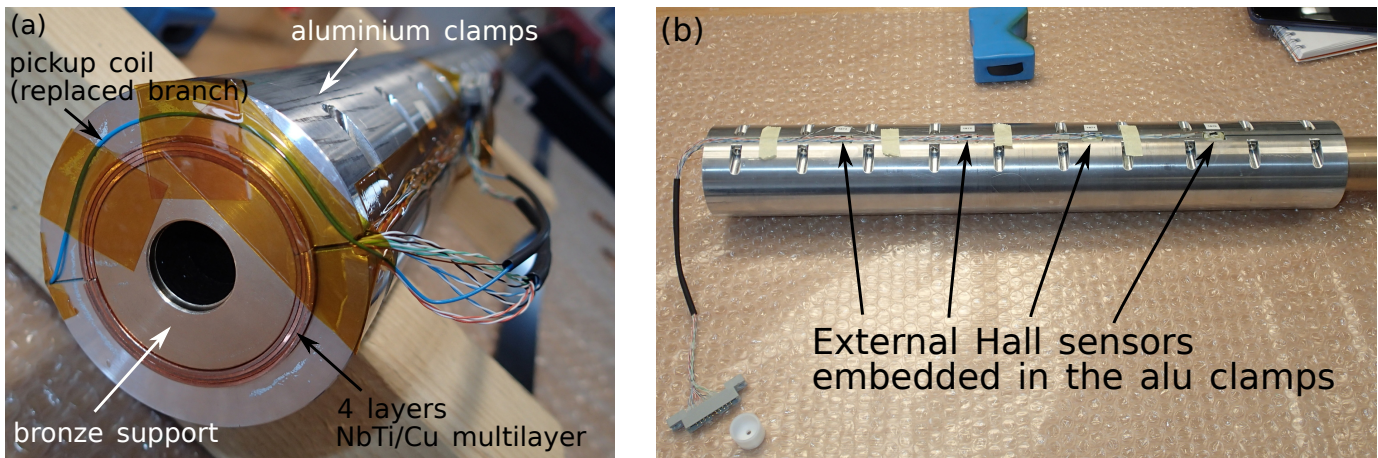


Fig. 2. The superconducting shield assembly. (a) End view showing the construction of the assembly and the pickup coil. (b) Positions of the external Hall sensors.

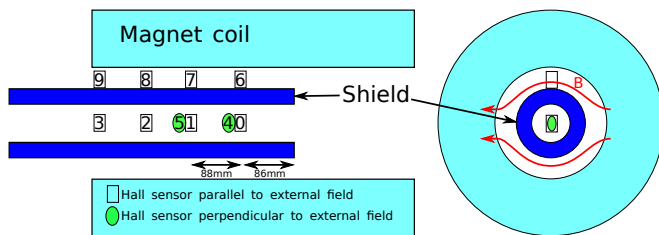


Fig. 3. Schematic layout of the experimental setup and the positions and numbering of the Hall sensor slots. Not to scale! The red arrows indicate the induction lines in the presence of the shield.

addition, the different layers could not be perfectly aligned during the assembly. The cuts in the different layers had slightly different orientations, also varying with the axial position. The tested configuration is therefore that shown in Fig. 1(b).

The half cylinders were clamped between a bronze tube support (ID/OD=18/41 mm) and half-cylindrical aluminium clamps, as shown in Fig. 2. Calibrated high-sensitivity Hall sensors (Arepec HHP-NP) were installed into slots of the aluminium clamps to measure the external magnetic field, with a parallel orientation. The same type of Hall sensors were mounted to a delrin rod, which was inserted into the bronze support tube. These sensors were aligned both parallel and perpendicularly to the external field. The layout and the numbering scheme of the Hall sensors is shown schematically in Fig. 3. The active spot of the external Hall sensors was about 2.6 mm away from the outer surface of the shield. The sensitivity of the individual sensors was between 150-200 mV/T at 4.2 K, allowing the measurement of fields below the mT scale using sensitive voltmeters. The sensors were driven by 20 mA (Current Generator type Keithley 6221) connected in series. The current and voltage measurement leads of the sensors were twisted wire pairs, and the series connection was done at an external patch panel, thereby avoiding that the series of the sensors acts as a large inductive pickup coil. The voltage of the sensors was read out by digital multimeters (Keithley 2000) and recorded by a computer at a

sampling rate of 10 Hz. The wires of sensor #6 got broken during cool-down, and this sensor was therefore not used in the analysis. Sensors #6 and #7 are in the full field region of the magnet, and measured equal values in earlier tests with an MgB₂ shield. Sensors #8 and #9 are in the fringe field and measure lower values.

A thin pickup coil was installed around the shield in the gap between the two aluminium clamps, as visible in Fig. 2(a). Unfortunately, one half of the coil was crashed between the half-cylindrical sheets, and short-circuited to them. This half was replaced by the blue wire taped to the outside surface of the clamps in the midplane. The other, original branch of the coil is hardly visible in the figure among the wires of the Hall sensors. The purpose of this coil was to pick up sudden changes of the external magnetic field in case of a flux jump, measure its time difference with respect to the signals of the internal Hall sensors, and ultimately to evaluate the feasibility of this method as an early diagnostics of flux jumps, to safely abort the beam before the penetrating field has fatal consequences. The voltage measured at the two terminals of the pickup coil was measured by a fast digital integrator (FDI v3 [7]), and recorded by a computer at a sampling rate of 1 kHz.

The shield was installed into the bore of a spare LHC MCBY dipole corrector magnet, as shown in Fig. 4. The magnet has two large apertures (70 mm), powered independently. Without the shield this magnet creates a high-quality transverse dipole field, perpendicular to its axis. The magnet has a nominal field of 2.5 T at 4.5 K and 72 A [8], but the achievable field in the presence of the shield is higher. The length of the shield was chosen initially such that it extends beyond the fringe fields of another, short but large-aperture magnet at both ends. Unfortunately, this magnet was not available anymore and the magnetic length of the MCBY magnet (0.899 m) exceeded the length of the shield. The shield was therefore installed asymmetrically into the magnet, with one of its ends being outside of the fringe field, so that eventual effects due to the shield's open end being exposed to the strong field can be identified. The full setup was installed in

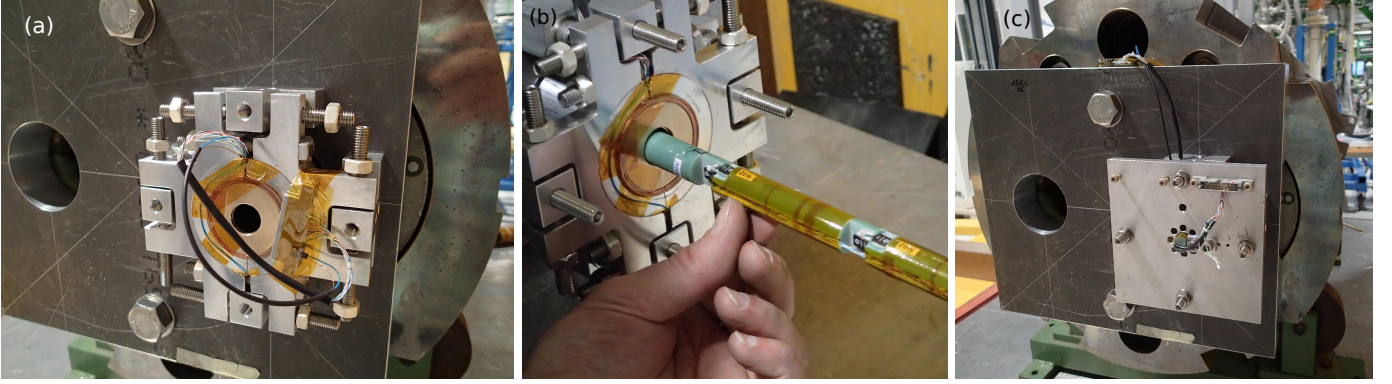


Fig. 4. The shield installed in one of the two apertures of the magnet. (a) Clamps to align the shield's position and orientation. (b) Delrin rod with the Hall sensors. (c) End plate to hold the shield in the magnet against the repulsive magnetic forces.

the Siegtal cryostat of the SM18 facility of CERN, and fully immersed in liquid helium.

III. NUMERICAL METHODS

Two different 2-dimensional finite element simulation models were used to reproduce the experimental results. (i) Campbell's model [9] is a static model which directly calculates the approximative steady state of Bean's critical state model [10], obtained by a direct ramp from a virgin state. This method is fast and therefore adequate for parameter scans and optimization. It is not applicable for time-dependent phenomena, such as relaxation, and for magnetic field ramps with different directions, i.e. hysteresis simulations. For the non-symmetrical cases extra parameters (the values of the vector-potential A_z in the interior of the bulk superconductors) were introduced and solved for by requiring that the current density integrated over the cross section of each superconducting piece be zero, as described in [1]. (ii) A time-dependent eddy current simulation using the power-law E-J characteristics $E = E_0 \cdot [J(B)/J_c(B)]^n$, with $E_0=100 \mu\text{V/m}$ and $n=100$, typical values used in the literature [11]. In both cases the critical current density of the shield material was taken from Figure 2 of reference [6], multiplied by the NbTi filling factor of 0.36 (transport current parallel to the rolling direction of the sheet, $350 \text{ }^\circ\text{C} \times 672 \text{ h}$ heat treatment, dashed line and open symbols).

IV. RESULTS

After the installation and cool-down of the setup, initial tests of the magnet, its power supply and quench protection system were carried out, which included fast ramp-ups of the magnet current, and fast energy extraction. These have led to flux jumps in the shield, or the quench of the magnet, which in turn induced a flux jump in the shield. The first measurement of the shield was carried out starting from this state with trapped magnetic field. Figure 5 shows the magnetic field levels after the subtraction of the trapped field offset (indicated in the legends). A strong penetration of the changes in the external field started during the ramp after the 6th plateau (starting at around 22 minutes). It must be noted that this penetration is smooth and relatively slow yet. The avalanche-like sudden

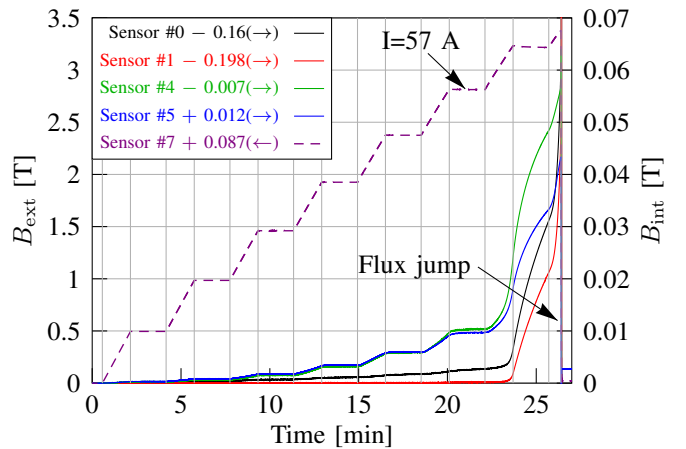


Fig. 5. Color online. Magnetic field measured by the external (dashed lines) and internal (solid lines) Hall sensors, after offset (trapped field) subtraction (see text for details). The vertical lines indicate the start and end of the ramps. Plateaus correspond to integer multiples of 9.5 A magnet current. Ramp rate is 0.1 A/s. Arrows in the legend indicate the vertical axis.

collapse of the shielding currents (flux jump) occurred at about 26 minutes. This triggered the magnet protection system and the magnet current was very quickly ramped to zero, terminating the measurement cycle.

In order to eliminate the trapped field from the shield it was warmed up above its critical temperature. The signal of the Hall sensors was monitored during the warm-up, and clearly indicated the transition of the shield to normal-conducting state by the sudden disappearance of the trapped field. The temperatures shown by the sensors attached to the magnet were around 50 K, when cool-down in zero field started again. Even though electric heaters were attached to the magnet, the complete cycle took almost 24 hours due to the long time needed to evaporate liquid helium from the large cryostat, and the large heat capacity of the 1.2 tons magnet. Testing the ultimate shielded field starting from a virgin state would have led to another full penetration and the loss of another 24 hours due to the subsequent thermal reset cycle. Due to the limited time for the experiment, this test was omitted. Subsequent measurements from a virgin state were limited to a magnet current of 55 A, slightly below the value at the last

stable plateau (57 A) in Fig. 5, hoping and then finding that this is still below the penetration limit. The following results indicate therefore only a lower limit of the shielding capability of the shield. Figure 6 shows the magnetic field measurements during a cycle between ± 55 A, starting from the virgin state. At the highest current the external magnetic field measured by sensor #7 was ± 2.7 T. According to a 2D finite element simulation of the experimental setup (taking into account the exact coil and yoke geometry of the magnet and the shield) this corresponds to a magnetic field of about 3.1 T at the shield's surface. Among the internal Hall sensors (solid lines of Fig. 6) the ones with perpendicular orientation (#4 and #5) measured by far the largest field, up to 12.5 mT. This corresponds to an attenuation of 4.6×10^{-3} . Sensor #0, oriented parallel to the external field, measured only 3 mT, corresponding to an attenuation of 10^{-3} . This value is 5 times more than that resulting from a 3D simulation assuming a perfect diamagnet shield. Field leakage of parallel orientation at this position is due to this sensor being close (86 mm) to the open end of the shield with a comparably large aperture (41 mm). Inner sensor #1 (at the same axial position as the external sensor #7) measured a magnetic field only below 0.1 mT, which corresponds to an attenuation of 4×10^{-5} , already acceptable for the intended application. The corresponding value in the 3D simulation with a perfect diamagnet shield was zero within the precision of the simulation. At the end of the cycle both the external and the internal sensors show the presence of trapped magnetic field.

Figure 7 shows the results of a 2D simulation using Campbell's method for the experimental geometry with a cut of 0.5 mm and rotation of the shield by 1.5° . The dominant field component is perpendicular to the external field: the field levels inside the shield are 15 mT and 0.4 mT in the perpendicular and parallel directions, respectively. This is a hint that the observed leakage magnetic field can be attributed to the actual shield geometry with unprecise alignment, as suggested in Fig. 1(b), and not limited by material performance. An ideally arranged configuration [such as that shown in Fig. 1(c)] extending safely beyond the fringe field of the magnet would presumably perform at least as well as suggested by sensor #1, i.e. with an attenuation of better than 4×10^{-5} .

Figure 8 shows the magnetic field measured by the external sensor #7 on the two plateaus, shifted on the horizontal axis to match their starting points. The behaviour is very similar in the two cases. The relaxation is about 0.26% over 7 minutes, and saturates with time.

Following this cycle, the shield was cooled down to 1.9 K without a thermal reset cycle. The magnet current was linearly ramped to 38, 47.5, 55, 57, 59 A in a sequence. Figure 9 shows the magnetic field measured inside and outside the shield. Small offsets at the beginning are due to the trapped field. In contrast to the results at 4.2 K, the inner sensors showed no creep on the plateaus, and the maximum variation of their values was significantly less, 4.5 mT. For sensor #0 this variation was 1.5 mT, only 2.5 times higher than the leakage field in the 3D simulation assuming a perfect diamagnet shield. These reflect the smaller relaxation of the shielding currents and the higher value of the critical current at

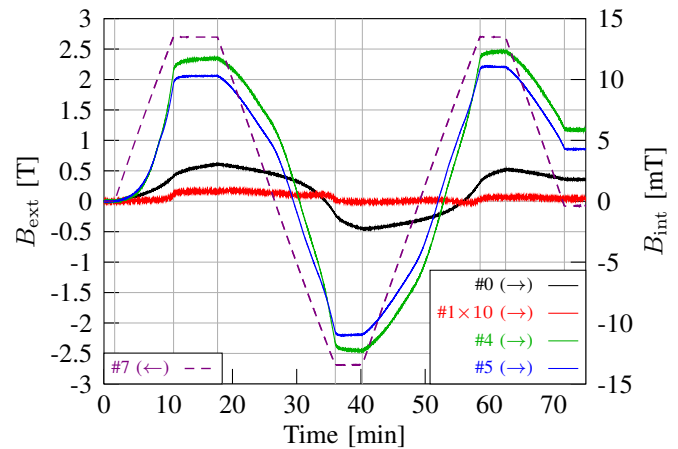


Fig. 6. Color online. Internal and external magnetic fields measured during a cycle between ± 55 A starting from a virgin state. The legends indicate scaling factors.

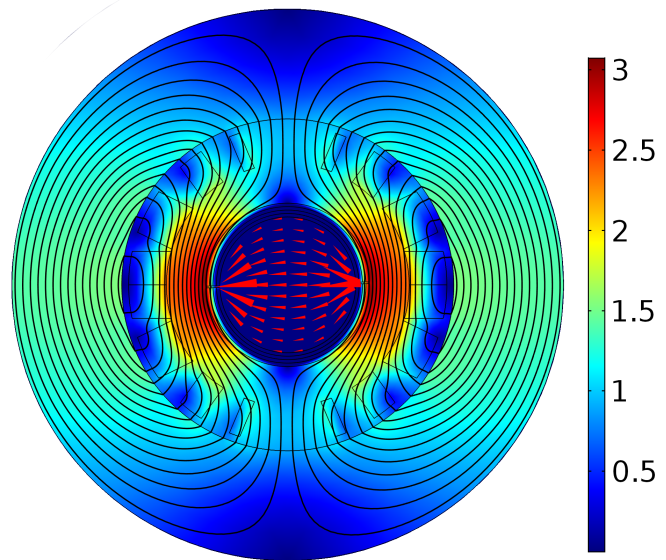


Fig. 7. Color online. Finite-element simulation of the cut shield geometry with improper alignment. Black lines and red arrows indicate the magnetic field.

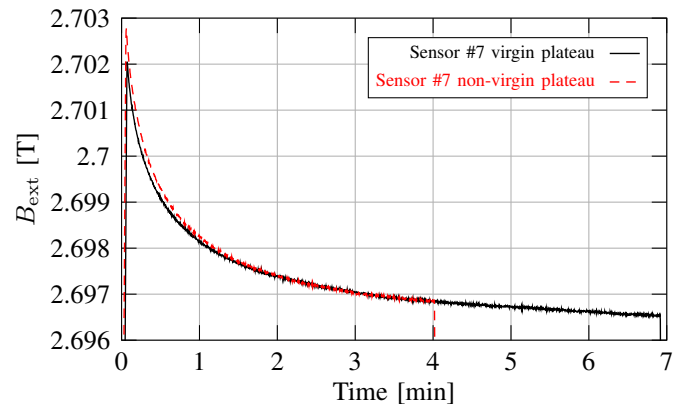


Fig. 8. Comparison of the field measured by sensor #7 on the two plateaus.

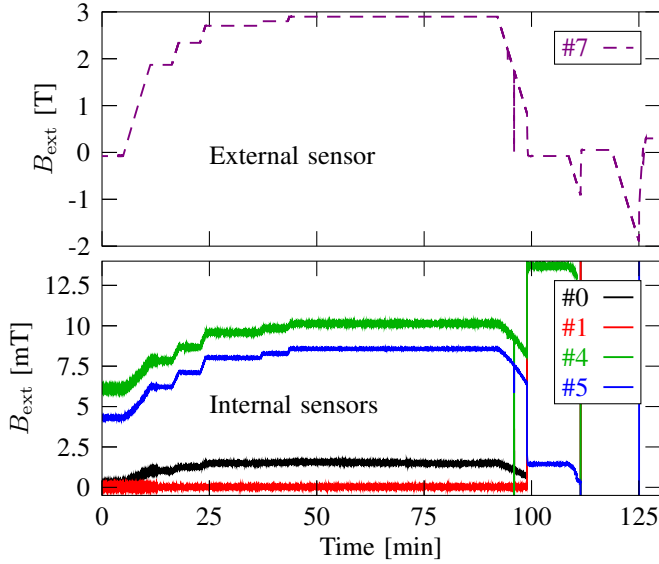


Fig. 9. Color online. Magnetic field measurements at 1.9 K.

lower temperatures. Rather than testing the ultimate shielding performance of the shield at 1.9 K which would have lead to the penetration of the field into the shield's interior (either smoothly or as a flux jump), the magnet current was ramped down to zero in order to test the stability of the shield during a full cycle. A flux jump occurred when reaching about 0.7 T outside the shield. Further attempts to ramp up the magnet current again were hindered by persisting flux jumps. This phenomenon was similar to the observations with an MgB_2 shield at 4.2 K in a similar measurement [12]. In spite of the better shielding performance, superfluid helium temperatures are therefore not applicable for the high-field septum concept.

A quantitative study of the effect of trapped field for the realistic configuration of a SuShi septum is clearly beyond the scope of the present paper. Here we only demonstrate a possibility to eliminate this effect using a kind of 'degaussing' cycle (Fig. 10) at 4.2 K. The shield started from a virgin state after a thermal reset. The magnet current was ramped to 54 A and then back to zero. This corresponds to the solid black line $O-A-B$ in Fig. 10(b). At zero current the trapped field at the position of sensor #7 was 75 mT. A second ramp to 54 A (green dotted line $B-A$) had a trace different from the virgin curve but reached the final endpoint A as before. This illustrates the effect that exposures to fields up to or beyond the highest level reached before erase the magnetic history of the shield. A double-ramp to -54 A and 54 A traced the full, symmetric hysteresis loop (red dashed line $A-C-A$). A degaussing cycle with alternating polarities and decreasing amplitudes (solid blue line $A-D-E-F-G-O$) brought the shield back to the same effective magnetic state O as the starting point. The trace of the last ramp to 54 A (green dashed line) seems to slightly deviate from the virgin curve, but reaches the same endpoint A . The phenomenon was simulated using the time-dependent method and the same magnet current profile as that used in the experiment, except on a shorter timescale (10.8 A/s ramp rate, no plateaus), to

make the simulation run faster. Figure 11(a) shows the fine alternating pattern of the persistent currents and magnetic field after the degaussing cycle. The majority of the induction lines are closed within the shield. The stray field at the position of the Hall sensor is negligible. These results illustrate that the magnetic state of the shield is reset only at the effective level which, nevertheless, is sufficient for the intended application. The microscopic field pattern still carries information about the shield's magnetic history. Figure 11(b) shows the same hysteresis loops as in Fig. 10(b). The last ramp to 54 A (blue dashed line) deviates from the virgin curve, but touches the previous endpoints of the degaussing cycle G and E . This is due to the fact that the persistent current layers are erased in a sequence when the field penetrates again through the wall of the shield. A magnetic state identical to a previous one will be reached when a complete persistent current layer is erased. The differences between the simulation and experimental results are probably due to the faster ramp rates in the simulation (less time for relaxation, higher instantaneous induced currents), the approximative nature and the non-optimized parameters of the E-J power law, and the difference between the $J_c(B)$ curve used in the simulation and in reality. The simulation nicely describes the experimental findings qualitatively and helps to understand the underlying phenomena. Since a time-dependent nonlinear eddy current simulation is computationally expensive, optimization of the parameters was not attempted.

The slow data acquisition rate (10 Hz) of the Hall sensors read out by the multimeters did not allow to measure eventual time differences below 100 ms between the signals of the Hall sensors and the pickup coil in case of a flux jump. For this measurement the Hall sensors #1 (inside the shield) and #7 (outside the shield) were connected to two other channels of the FDI with a gain of 2 to obtain the same 1 kHz sampling rate as for the pickup coil. At 4.2 K the magnet current was ramped to 57 A with a ramp rate of 0.5 and 1 A/s. The shield was stable and no flux jump occurred. When higher ramp rates were set, the power converter tripped. A flux jump provoked by higher magnet currents would have been preceded by a smooth penetration, as in Fig. 5 and in [2]. Given the apparent stability of the shield against flux jumps at the intended field levels, in a realistic scenario an eventual flux jump would be caused by an external perturbation, like energy deposition due to beam loss. In this case a flux jump would occur suddenly and directly from a perfectly shielding state. In order to trigger a similar situation, the shield was cooled down to 1.9 K. Figure 12(a) shows the usual Hall sensor curves as a function of time. As expected, a flux jump occurred at $t=1112$ s. The signals recorded by the FDIs are shown in Figure 12(b). A clear peak in the signal of the pickup coil precedes the peak measured by the external Hall sensor by about 10 ms, and the departure of the internal Hall sensor's signal by about 15 ms. This time interval seems to be safe to trigger an emergency beam abort in the ring. Since the pickup coil encircles the whole shield, its inductive signal records flux jumps starting at any point along the shield. In fact, the recorded shape of the peak might indicate flux jumps starting at two different locations, with a small time difference, although this statement is rather speculative. In

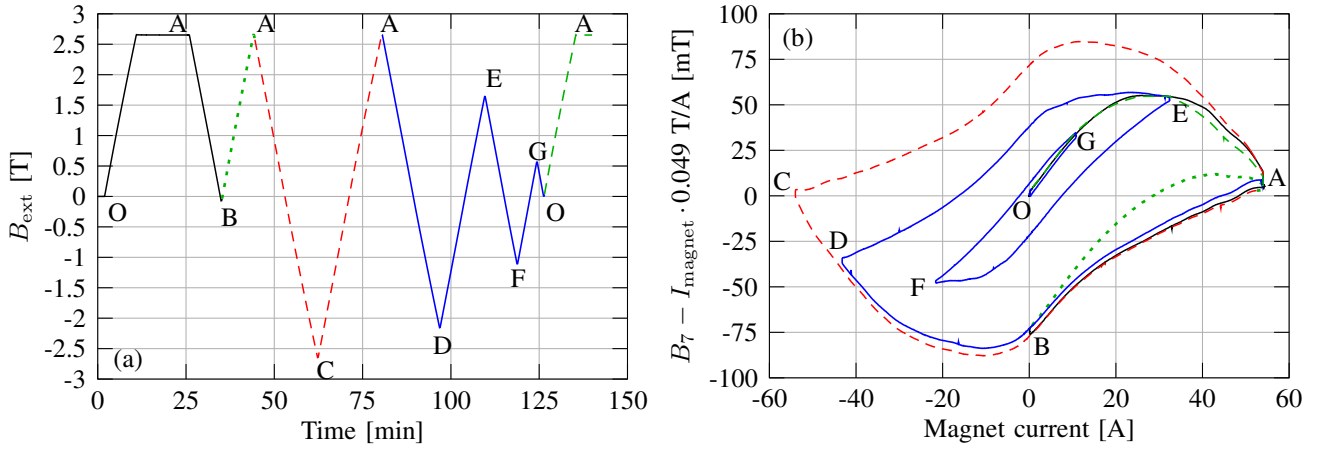


Fig. 10. Color online. Demagnetization of the shield. (a) External magnetic field measured by sensor #7 as a function of time. (b) Deviation of the external magnetic field from a linear behaviour, as a function of magnet current.

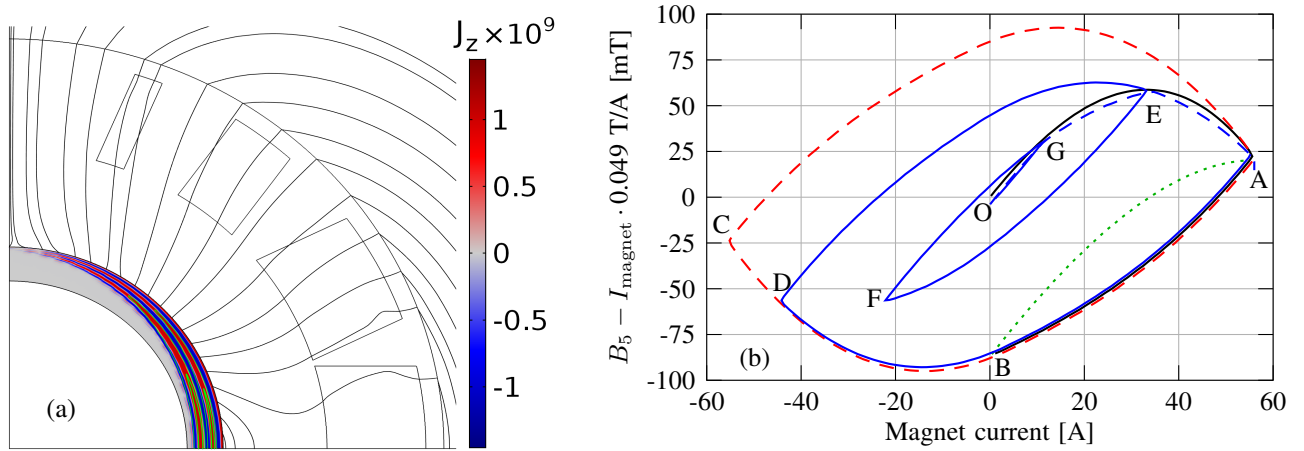


Fig. 11. Color online. (a) Simulated pattern of the magnetic field after a degaussing cycle. Color scale indicates the persistent currents J_z . Black and green lines indicate the induction lines, color is only for better visibility. The distribution of the induction lines was chosen manually for illustration purposes, their density does not reflect actual field strength. (b) Reproduction of the measured hysteresis cycle [Fig. 10(b)] by simulation

contrast, the Hall sensors are recording magnetic field levels at well defined spots inside and on the outer surface of the shield. Time differences between the pick-up coil and the Hall sensors might therefore be a purely geometrical effect, caused by the propagation of the instability along the axis of the shield. However, since the two recorded Hall sensors are at the same longitudinal positions, the observed time difference between their signals can be attributed to the retarding effect of the eddy currents induced in the shield and its bronze and aluminium support structure. The quantitative results are therefore clearly a function of the specific geometry and the amount of conductor material around the circulating beam, which should be maximized in the final design.

V. CONCLUSIONS AND OUTLOOK

The Future Circular Collider project is seeking for novel concepts to manipulate its proton beam of unprecedented energy. One of the challenges is the construction of a high-field septum magnet with a field of at least 3 T, and an apparent septum thickness below 25 mm. One of the proposals is to realize this device using a combination of a passive

superconducting shield and a special superconducting magnet, nicknamed as a SuShi septum. This paper reported on the magnetic shielding properties of a candidate superconducting shield material, a 0.8 mm thick NbTi/Nb/Cu multilayer sheet. A cylindrical shield, constructed from 4+4 layers of this material, in the form of two half-cylinders, with a total wall thickness of 3.2 mm could support 3.1 T on its surface, in accordance with the results of [2], even though the shield's construction was different. We estimate that with 5 layers and a total thickness of 4 mm only, the shield could support 3.2 T with a safety margin, the current value used in the FCC conceptual design report for this type of device. Together with an additional support of 11 mm thickness and the beam pipes and beam screens the apparent septum thickness would be below the target value. The shield material is ductile and easy to form and handle. It was stable against spontaneous flux jumps at 4.2 K, and survived magnetic cycles between opposite polarities without flux jumps. Relaxations of the shielding currents are at a tolerable level, and we have demonstrated a “degaussing” method to eliminate the effects of the field trapped in the shield's thick wall after high field exposures.

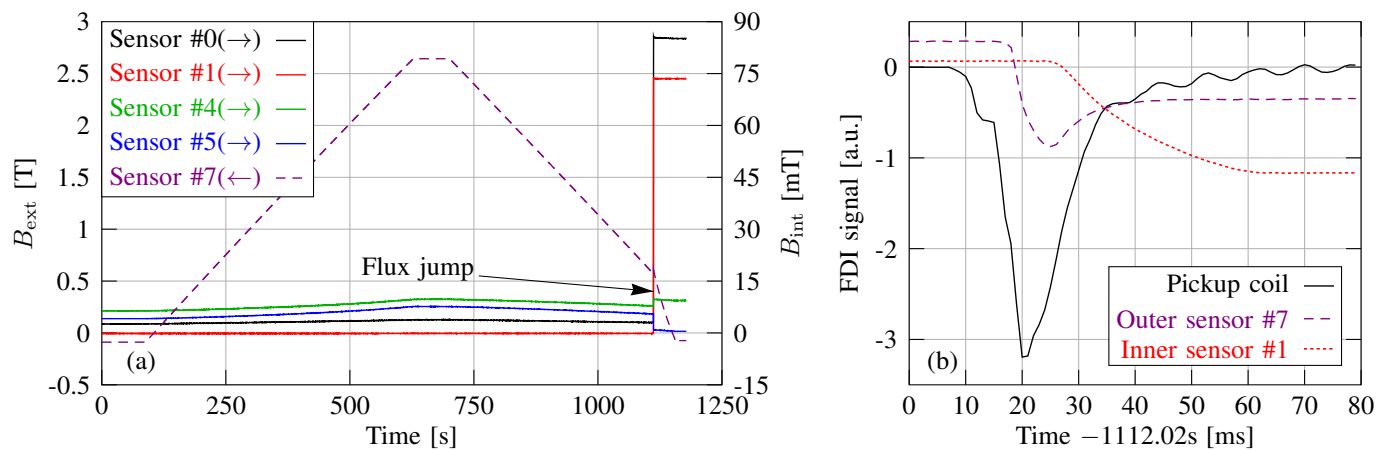


Fig. 12. Color online. Timing measurements of a flux jump at 1.9 K

Even though the shield's performance was better at 1.9 K in terms of shielding efficiency and relaxation rates, frequently occurring flux jumps make this temperature inapplicable. The observed properties of the material make it an ideal candidate for the realization of a SuShi septum magnet. Unfortunately the material is a discontinued product of Nippon Steel Ltd., and its availability is not clear even on the short term. The material for the reported tests was purchased from a small remaining stock of semi-finished products of the company, post-processed to the final thickness and specifications by a private company in Japan. If the material can be produced in larger quantities, the unit cost is expected to be reduced.

MgB₂, another candidate material, also demonstrated an excellent shielding performance in a similar test. It supported 3 T on its surface with a wall thickness of 8.5 mm, perfectly shielding its interior [12]. However, it suffered from flux jumps when the external field was ramped down to zero. This material is relatively cheap and easy to produce, and if the latter problem can be solved, it provides an alternative to the NbTi/Nb/Cu multilayer sheet. Flux jumps are one of the most important issues of this concept. Stability against this phenomenon requires careful manufacturing and processing of the material, and each shield must be tested to be "flux jump safe" before assembly into the setup.

Encouraged by these positive test results, a study is now underway to design and optimize a fully fledged demonstrator prototype, using a canted cosine theta-like magnet and a half-moon shaped shield [13]. Besides the demonstration of the achievable maximum field strength in a realistic configuration, this prototype would create a homogeneous field outside the shield, and it would allow the measurement of the field quality in the high-field region.

ACKNOWLEDGEMENTS

The authors would like to express their gratitude to the CERN TE-ABT group, the CERN SM18 team, the CERN magnetic measurements group TE-MSC-MM, Akira Yamamoto, Ikuo Itoh, Márta Bajkó, Ranko Ostojic, Frédéric Rougemont, Yannick Thuau. This project has received funding from the FCC Study Group, the European Union's Horizon

2020 research and innovation programme under grant agreement No 730871 (ARIES), and from the Hungarian National Research, Development and Innovation Office under grant #K124945.

REFERENCES

- [1] D. Barna, "High field septum magnet using a superconducting shield for the Future Circular Collider," *Phys. Rev. Accel. Beams*, vol. 20, no. 4, p. 041002, 2017. [Online]. Available: <http://link.aps.org/doi/10.1103/PhysRevAccelBeams.20.041002>
- [2] I. Itoh, T. Sasaki, S. Minamino, and T. Shimizu, "Magnetic shielding properties of NbTi/Nb/Cu multilayer composite tubes," *IEEE Trans. Appl. Supercond.*, vol. 3, no. 1, pp. 177–180, 1993. [Online]. Available: <http://ieeexplore.ieee.org/document/233699/>
- [3] I. Itoh, K. Fujisawa, and H. Otsuka, "NbTi/Nb/Cu Multilayer Composite Materials for Superconducting Magnetic Shielding," *Nippon Steel Tech. Rep.*, vol. 85, p. 118, 2002. [Online]. Available: <http://www.nssmc.com/en/tech/report/nsc/pdf/8522.pdf>
- [4] A. Yamamoto, Y. Makida, K. Tanaka, F. Krienem, B. Roberts, H. Brown, G. Bunce, G. Danby, M. G-Perdekamp, H. Hseuh, L. Jia, Y. Lee, M. Mapes, W. Meng, W. Morse, C. Pai, R. Prigl, W. Sampson, J. Sandberg, M. Suenaga, T. Tallierico, F. Toldo, K. Woodle, M. Green, I. Itoh, H. Otsuka, Y. Saito, T. Ozawa, Y. Tachiya, H. Tanaka, A. Grossmann, K. Jungmann, G. zu Putlitz, H. Deng, S. Dhawan, V. Hughes, D. Kwall, J. Pretz, S. Redin, E. Sichtermann, and A. Steinmetz, "The superconducting inflector for the BNL g-2 experiment," *Nucl. Instruments Methods Phys. Res. Sect. A Accel. Spectrometers, Detect. Assoc. Equip.*, vol. 491, no. 1-2, pp. 23–40, 2002. [Online]. Available: <http://linkinghub.elsevier.com/retrieve/pii/S0168900202012329>
- [5] Z. Y. Zhang, S. Matsumoto, S. Choi, R. Teranishi, and T. Kiyoshi, "A new structure for a magnetic field concentrator using NbTi sheet superconductors," *Phys. C Supercond. its Appl.*, vol. 471, no. 21-22, pp. 1547–1549, 2011. [Online]. Available: <http://dx.doi.org/10.1016/j.physc.2011.05.235>
- [6] I. Itoh and T. Sasaki, "Critical current density of superconducting NbTi/Nb/Cu multilayer composite sheets," *Cryogenics*, vol. 35, no. 6, pp. 403–404, 1995. [Online]. Available: [https://doi.org/10.1016/0011-2275\(95\)99821-0](https://doi.org/10.1016/0011-2275(95)99821-0)
- [7] P. Arpaia, L. Bottura, P. Cimmino, D. Giloteaux, A. Masi, J. G. Perez, G. Spiezia, and L. Walckiers, "A fast digital integrator for magnetic field measurements at cern," *Conf. Rec. - IEEE Instrum. Meas. Technol. Conf.*, no. April, pp. 67–71, 2006. [Online]. Available: <https://ieeexplore.ieee.org/document/4124277/>
- [8] S. O. Bruning, P. Collier, P. Lebrun, S. Myers, R. Ostojic, J. Poole, and P. Proudlock, "LHC Design Report Vol. 1 Chapter 8 - Insertion Magnets," CERN, Tech. Rep., 2004. [Online]. Available: https://edms.cern.ch/ui/file/445847/5/Vol_1_Chapter_8.pdf
- [9] A. M. Campbell, "A new method of determining the critical state in superconductors," *Supercond. Sci. Technol.*, vol. 20, pp. 292–295, 2007. [Online]. Available: <https://doi.org/10.1088/0953-2048/20/3/031>

- [10] C. P. Bean, "Magnetization of high-field superconductors," Rev. Mod. Phys., vol. 36, no. 1, pp. 31–39, 1964. [Online]. Available: <http://journals.aps.org/rmp/pdf/10.1103/RevModPhys.36.31>
- [11] S. Russenschuck, Field computation for Accelerator Magnets. WileyVCH Verlag GmbH & Co, 2010.
- [12] D. Barna, "First experimental results with the superconducting shield (sushi) prototypes." <https://indico.cern.ch/event/556692/contributions/2488390/attachments/1468982/2272308/barna-sushi.pdf>, 2017, talk presented at the FCC Week 2017, Berlin.
- [13] D. Barna, "Superconducting shield (sushi) septum - towards a full prototype." <https://indico.cern.ch/event/656491/contributions/2947265/attachments/1630674/2599275/barna-sushi-fcc-week-amsterdam.pdf>, 2018, talk presented at the FCC Week 2018, Amsterdam.